Kadotani, Ken; Fujita, Ichiro; Matsubara, Takayuki; Tsubaki, Ryota

Analysis of Water Surface Osccilation at Open-Channel Side Cavity by Image Analysys and Large Eddy Simulation

ANALYSIS OF WATER SURFACE OSCCILATION AT OPEN-CHANNEL SIDE CAVITY BY IMAGE ANALYSYS AND LARGE EDDY SIMULATION

Ken Kadotani[1], Ichiro Fujita[2], Takayuki Matsubara[3] and Ryota Tsubaki[4]

[1] Graduate student, Department of Civil Engineering, Kobe University
Rokkodai-cho, Nada-ku, Kobe, 657-8501, Japan, e-mail: 065t110n@stu. kobe-u.ac.jp
[2] Professor, Department of Civil Engineering, Kobe University
Rokkodai-cho, Nada-ku, Kobe, 657-8501, Japan, e-mail: ifujita@kobe-u.ac.jp
[3] Graduate student, Nitto Denko Corporation
Herbis Osaka, 2-5-25,Kita-ku, Osaka, 530-0001, Japan, e-mail: ifujita@kobe-u.ac.jp
[4] Researcher, Department of Civil Engineering, Nagoya University
Furo-cho, Chikusa-ku, Nagoya, 464-8603, Japan, e-mail: r.tsubaki@civil.nagoya-u.ac.jp

ABSTRACT

When a side cavity structure is installed in a relatively narrow open-channel, appreciable surface oscillation sometimes takes place with the increase of the Froude number. Once this type of oscillation occurs in the actual river section, unexpected overflow from a channel might be generated, causing flooding in the worst situation. Therefore, estimation of oscillation intensity and oscillation type at a side cavity is necessary to design a safe channel section intended to improve the accessibility to the water front and riverside landscape. In order to find the type of oscillation we performed laboratory experiments for a wide range of aspect ratio of the rectangular side cavity. Subsequently, we conducted a numerical simulation with the large eddy simulation (LES) model that allows the water surface variation using a density function. The characteristics of surface oscillations were examined by using the proper orthogonal decomposition (POD) method. It was found that the surface oscillation can be categorized into several types, one of which exhibits a significant resonance pattern with complicated correlation between surface oscillation and velocity distribution.

Keywords: side cavity, LES, surface oscillation, stereoscopic surface measurement, POD

1. INTRODUCTION

It is commonly observed that side cavity section is installed in a river for the purpose of improving the accessibility to the river water front especially in normal flow conditions. The installation of such side cavity section would have no influence to the main stream when the scale of the side cavity is relatively smaller than the main channel width. However, as is found in small scale urban rivers in Japan, relatively large scale side cavity structures are occasionally installed in a river reach flowing through urban areas for attracting people to the river itself. It has been reported through the experimental investigations (Fujita et al. 2001, Kimura and Hosoda 1997 and Tsubaki et al. 2004) that unexpected water surface oscillation is generated at such river sections for specific hydraulic and geometric conditions. Once such oscillation takes place in actual river flow situations, overflow of the main flow to the inland area might occur. In fact, inundation of downtown area actually occurred in a river flowing in Kobe city, which was considered to be the effect of a relatively large side cavity installation. Therefore, in order to design an appropriate channel with such river structure, estimation of river surface oscillation structures becomes necessary. In the light of such background, the

authors have analysed the flow with a rectangular side cavity by using a shallow water equation model (Tsubaki and Fujita 2004). However, the flow within a side cavity inherently exhibits three-dimensional flow features which cannot be explained in detail by a shallow water model. Three dimensional calculations for a side cavity flow are already performed by Yano and Nezu (2004) using a large eddy simulation (LES) model with the volume of fluid (VOF) treatment of water surface, with the results that large-scale turbulent vortices were reproduced by LES comparable to those measured using the particle image velocimetry (PIV) method. In this research, we developed an LES model capable to represent water surface variation with a density function and applied it for the analysis of surface oscillation modes at the side cavity section.

2. EXPERIMENTS

Experimental setup

In the experiment, distribution of water surface level at the side cavity section is measured stereoscopically by using two sets of video cameras and a projector as shown in Figure 1. The main channel width is 10cm and the water depth is kept constant at 4cm. For a two sets of the Froude number of the main channel, 0.6 and 0.8, the side cavity length was varied between 25cm and 35 cm and its width was varied between 5cm and 10 cm. The water color is made white so that the projected pattern appears just at the water surface. The surface velocity was measured by adding powdered charcoal from the upstream section. An example of visualized surface image is shown in Figure 2. The detailed surface level variation was measure efficiently by the method proposed by Tsubaki and Fujita (2005). The projected

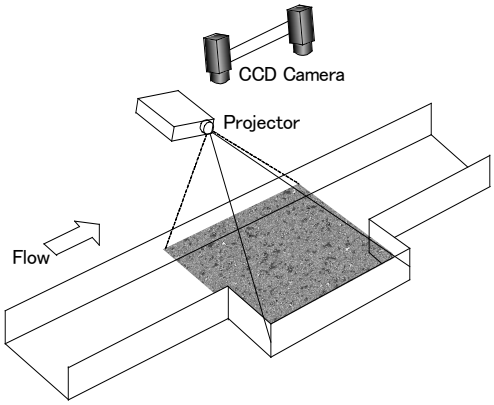

Figure 1 Experimental setup

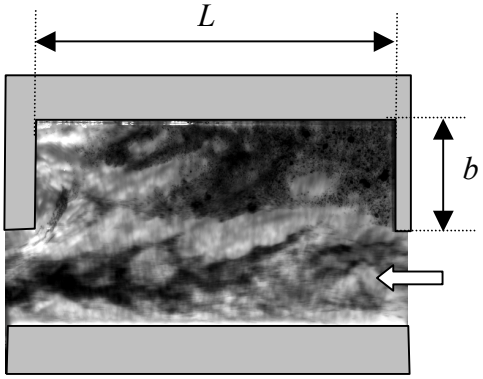

Figure 2 Visualized surface image

pattern together with the charcoal power successfully visualizes the instantaneous surface variation stereoscopically viewed from above the surface. On the other hand, surface velocity distributions are measured by tracking the movement of charcoal power by PIV. With the above combination of surface measurements, it becomes possible to measure surface level and velocity distribution simultaneously.

Surface oscillation types

The measured data of surface variation are analyzed using POD analysis in order to pick up the representative mode of oscillation. From the comparison of the mode with the maximum contribution to the oscillation, the surface oscillation was categorized into four types as illustrated in Figure 3.The circles shown in the figure correspond to the locally

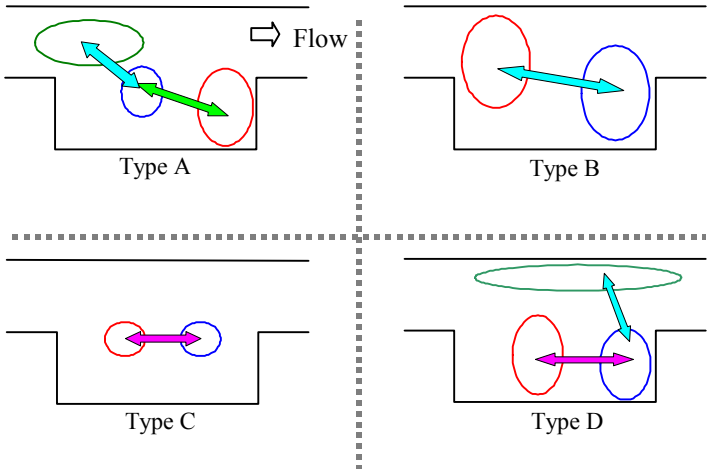

Figure 3 Four types of oscillation

oscillating zones. Each type has the following features:

Type A: intense oscillation in shear layer, upstream main channel and lower cavity corner

Type B: seiche-like oscillation between upstream main channel and lower cavity corner

Type C: weak oscillation along the shear layer

Type D: intense oscillation within cavity and the opposite main channel

As a representative case for comparison, we selected the following cases for each type:

Type A : Fr=0.6, L=35cm, b=10cm,

Type B : Fr=0.8, L=35cm, b=10cm,

Type C : Fr=0.6, L=30cm, b=10cm, and

Type D : Fr=0.8, L=30cm, b=10cm.

Here L stands for the length of the side cavity and b the side cavity width. In the following discussion, we use these cases for comparison.

3. NUMERICAL SIMULATION AND DISCUSIIONS ON OSCILLATION

Large eddy simulation model

The developed model is based on the large eddy simulation model that uses a density function for representing the water surface; therefore the calculation is performed in the air phase as well as water phase. Typical numbers of the grid are 155 in streamwise direction (155cm), 25 in horizontal direction in the main channel (10cm), from 15 to 25 in horizontal direction within the side cavity (6-10cm), 28 in vertical water phase (4cm) and 12 in vertical air phase (about 2cm). A periodical boundary condition is applied in the main channel. The Froude number was given by changing the channel slope to an appropriate value.

Comparison of water surface fluctuation intensity distribution

In order to evaluate the simulation model, the intensity distribution of water surface oscillation are compared in Figure 4 for one of the cases of type D, Fr08L30b10, in which case significant oscillation in spanwise and longitudinal directions is observed. Although the surface oscillation indicates complicated pattern with three local large peaks, i.e. along the interface between the main channel and the side cavity zone, at the lower end corner of the side cavity and near the side wall of the main channel, the simulated result agrees fairly well with the experiment except the level of intensity. This indicates that the developed model is capable to simulate the pattern of the surface oscillation.

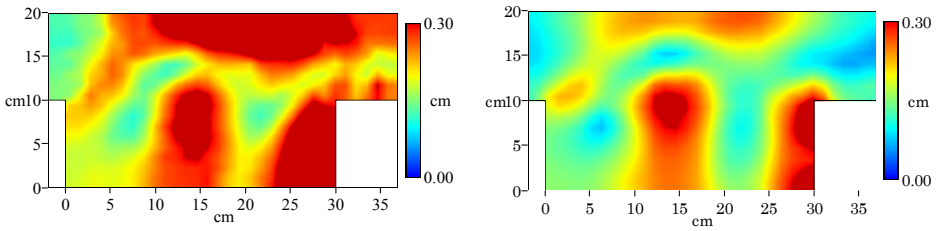

(a) Experiment (b) LES

Figure 4 Intensity of water surface oscillation (Type D: case Fr08L30b10; Fr=0.8, side cavity length L=30cm, width of side cavity b=10cm)

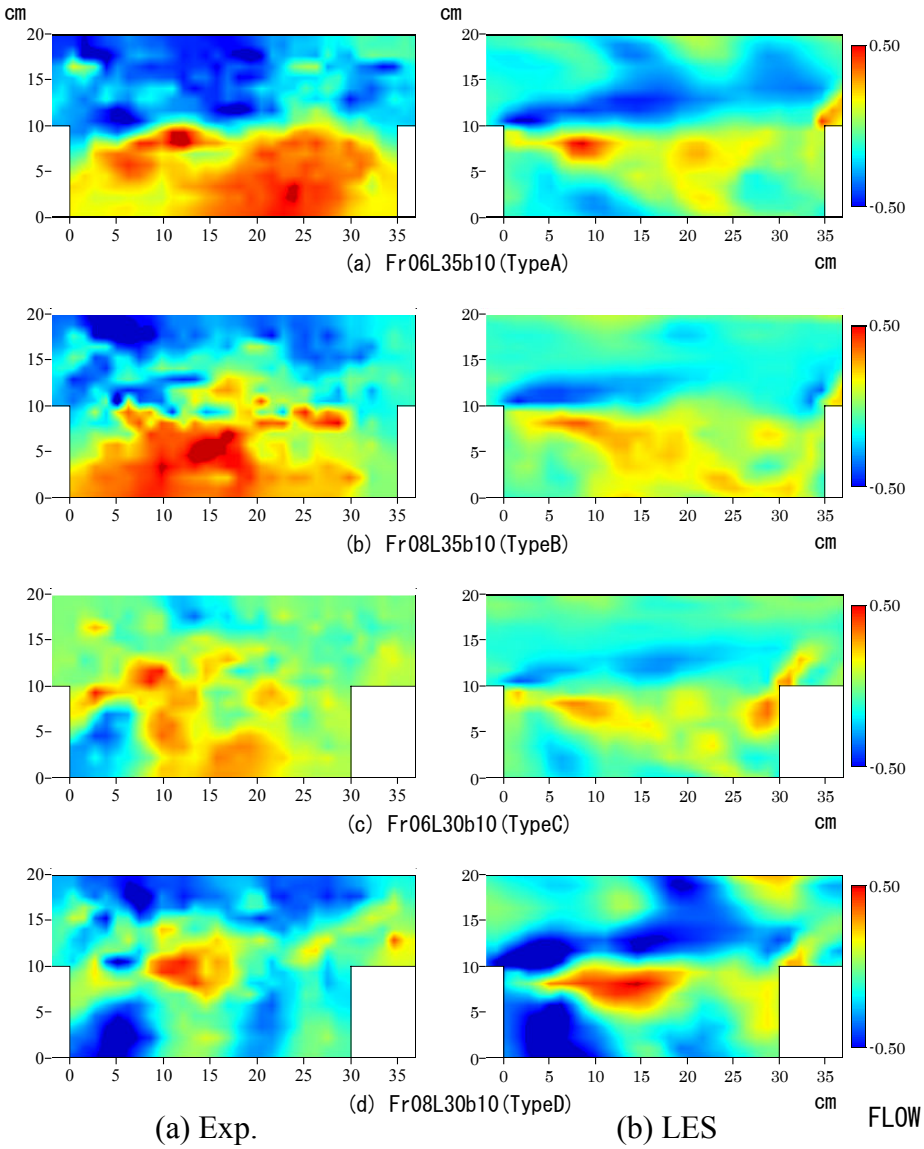

(a) Exp. (b) LES

Figure 5 Correlation between water surface level and streamwise velocity for various types of oscillations

Correlation between water-depth and velocity distributions

As mentioned previously, since the simultaneous measurement of surface flow and water depth is possible in the present experiment, the correlation between water depth and velocity component become possible. Figure 5 shows the comparison of the cross correlation distributions of water depth $h(t,x)$ and streamwise velocity component $u(x)$ defined by the following relation,

$$C_r(\mathbf{x}) = \frac{\sum_t [h(t,\mathbf{x}) - \bar{h}(\mathbf{x})][u(t,\mathbf{x}) - \bar{u}(\mathbf{x})]}{\sqrt{\sum_t [h(t,\mathbf{x}) - \bar{h}(\mathbf{x})]^2} \cdot \sqrt{\sum_t [u(t,\mathbf{x}) - \bar{u}(\mathbf{x})]^2}}. \quad (1)$$

In type A and type B, there appears a large positive correlation within the side cavity, while negative correlation zone is present in the main channel. This suggests that strong inflow from the main channel to the side cavity zone increase the water depth within the side cavity. On the other hand, in type D, there appears locally a positive correlation zone in the middle of the shear layer. The location of this peak zone coincides with one of the peaks indicated in Figure 4. This suggests that an intensive momentum exchange is evident at this anti-node location in type D. When we take scatter of the experimental results into account, the simulation model successfully reproduce the characteristics of the experiments fairly well.

POD analysis of surface fluctuations

Here, we pay attention to the water surface fluctuation more in detail by applying the proper orthogonal decomposition (POD) method to the experimental and numerical results. Figure 6 demonstrates the analysed results for experiments and simulations with oscillation patterns up to the third mode. Red and blue regions are antinodes of water surface oscillation with opposite phase, while green regions correspond to nodes with little surface fluctuation.

In the case of type A, the first mode shows three oscillation zones in the middle of the side cavity zone and their upstream and downstream zones with two nodes. The second mode includes two oscillation zones divided by the node in the middle of the channel. The third mode represents fluctuations along the shear layer developed between the main stream and the cavity regions. The numerical results for each mode almost agree with the experiments in this case.

In type B, the first mode shows streamwise oscillation that ranges in the entire zone divided by a node line normal to the flow direction. This mode is the origin of the seiche-like oscillation. The patterns of the second and the third modes are similar to those of the third and the second modes respectively, each having rather complicated node lines.

In type C, although agreement level between experiment and simulation is not so high, each results show oscillations within the side cavity zone in the first mode. In simulation the second mode presents oscillation between upper cavity corner and the lower main channel. This mode is not observable in the experiment; on the other hand local oscillations along the shear layer are captured in the experiment not appeared in simulation. Generally, the oscillation intensity itself is relatively lower that the other types and it can result in the less accurate measurement in this case. The type C, therefore, can be considered as a transient mode in between the other types.

Although the pattern of the first mode and the second mode is exchanged between experiment and simulation in type D, the corresponding mode yields a resembling pattern with each other. As will be explained in the subsequent discussion, since these two modes have the same oscillation period, they are taking a complementary role of the entire

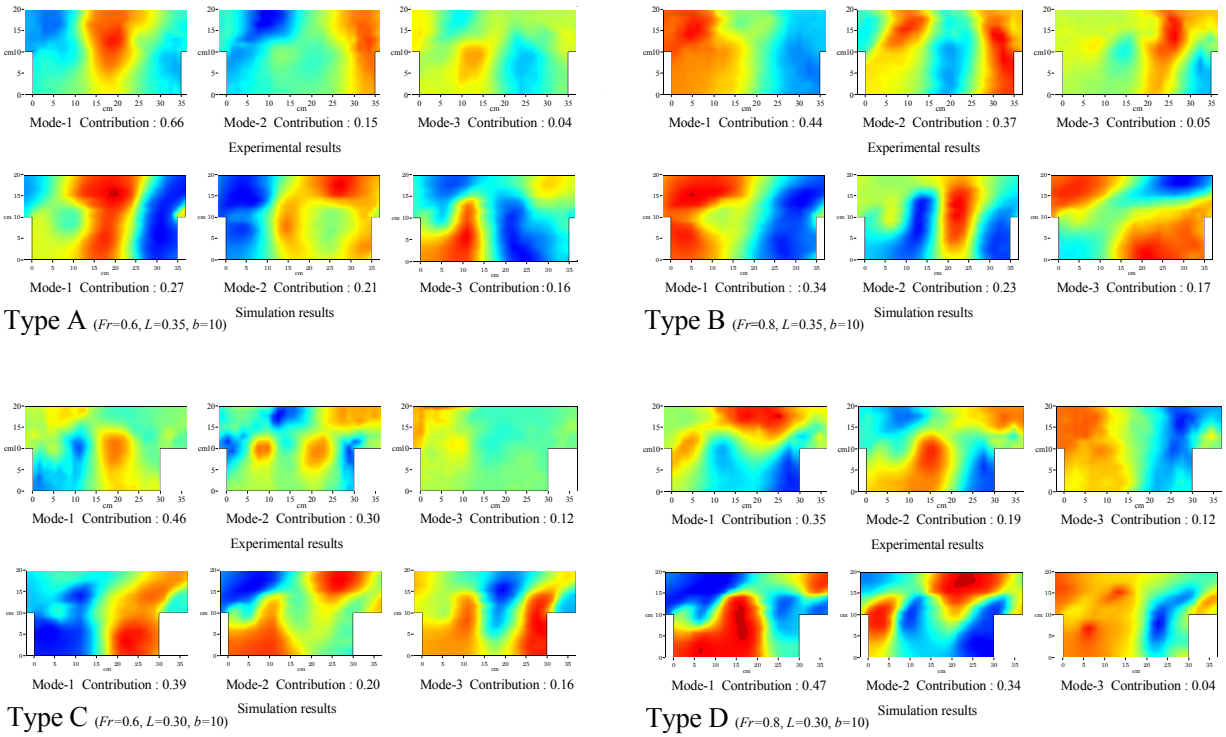

Figure 6 Mode of oscillation for each type analyzed by POD

oscillation.

Frequency characteristics of surface oscillation

In this section, frequency characteristics of surface oscillation are examined by comparing the POD results with several representative equations for surface oscillation. The possible oscillation period can be estimated from the following equations, i.e. with n the number of mode, h the mean depth and l_s the length scale,

1. closed seiche:

$$T = \frac{2l_s}{n\sqrt{gh}} \tag{2}$$

2. semi-close seiche:

$$T = \frac{4l_s}{(1+2n)\sqrt{gh}} \tag{3}$$

3. Rossiter's empirical equation with $M=Fr$, $\gamma=0.25$ and $\kappa=1/1.75$:

$$St = \frac{f_n l_s}{U} = \frac{n-\gamma}{M+1/\kappa} \tag{4}$$

Table 1 summarizes the first and the second peak periods for experiments and simulations obtained by spectral analysis with those calculated from the above equations. In the case of type A, the predominant period 1.18s is observed in simulation and experiment. This corresponds to the closed seiche period 1.12s with the side cavity length L as a length scale. There also appears other oscillation periods 2.27s and 2.13s, which are close to the period

Table 1 Comparison of predominant periods [s]

		Experiment		Simulation		Closed seiche		Semi-closed seiche		Rossiter	
		Mode1	Mode2	Mode1	Mode2	$L(n=1)$	$B+b(n=1)$	$L(n=1)$	$L(n=2)$	$L(n=1)$	$L(n=2)$
Type A	1st. Peak	2.27	1.19	1.18	1.18	1.12	0.64	2.23	0.74	2.92	1.25
	2nd. Peak	1.18	2.27	2.13	2.13						
Type B	1st.	1.96	1.96	1.92	0.60	1.12	0.64	2.23	0.74	2.37	1.02
	2nd.	2.27	2.27	1.43	0.85						
Type C	1st.	0.62	0.63	2.04	0.63	0.96	0.64	1.92	0.64	2.50	1.07
	2nd.	0.99	-------	0.63	-------						
Type D	1st.	0.71	0.71	0.75	0.75	0.96	0.64	1.92	0.64	2.04	0.87
	2nd.	0.56	0.56	-------	-------						

2.23s of semi-closed seiche period with n=1. The semi-closed seiche indicated here is the oscillation between the upper main channel and the lower corner of the side cavity. Therefore, type A includes mainly two kinds of seiche oscillation, closed seiche and semi-close seiche.
Type B seems to include the period close to the semi-closed seiche period 2.23s which can also be estimated from Figure 6. In the experiment, another period close to the Rossiter's frequency with n=1 is observed. The predominant period of type C is close to the closed seiche period 0.64s calculated using the maximum transverse width $B+b$ as the length scale. This value coincides with the semi-closed seiche with a length scale of L and n=2. Therefore, both streamwise and transverse seiche oscillations are superposed in type C. In contrast to the previous types, the peak period for type D, 0.71s in experiment and 0.75s in simulation, is extremely predominant than the other lower peaks. This peak period is close the closed seiche period with $B+b$ as the length scale and the semi-closed seiche period with a length scale of L, though not exactly the same as seen in type C. According to the oscillation pattern in Figure 6 revealed by POD, it is evident that the oscillation occurs in the upper and lower regions. Since the oscillations of the first and the second modes are shifted by $\pi/2$, the actual water surface oscillation seems to rotate within the region that encompasses the main channel and the side cavity zone.

4. INTERNAL FLOW STRUCTURE

As has been discussed previously, the LES mode developed by the authors is capable to represent the overall surface oscillation features. Hence, in the following discussions the simulated results are examined to investigate the relation between the surface oscillation and the internal flow structure at the side cavity.

Correlation between streamwise velocity and depth at the lower cavity corner

In the present analysis, the correlation between the three-dimensional streamwise velocity distribution $u(t, \mathbf{x})$ and the water depth fluctuation at the lower end corner of the side cavity $h_s(t)$ is investigated using the following cross correlation function,

$$C_r(dT,\mathbf{x}) = \frac{\sum_t [h_s(t)-\bar{h}_s][u(t-dT,\mathbf{x})-\bar{u}(dT,\mathbf{x})]}{\sqrt{\sum_t [h_s(t)-\bar{h}_s]^2}\cdot\sqrt{\sum_t [u(t-dT,\mathbf{x})-\bar{u}(dT,\mathbf{x})]^2}} \tag{5}$$

where $\mathbf{x}$ stands for the space coordinates (x,y,z) and dT the time lag between $h_s(t)$ and $u(t, \mathbf{x})$.

Figure 7 demonstrates the three-dimensional expression of the correlation field with dT =0. The red ball indicates the positive h_s-u correlation and the blue one the negative correlation, with their size corresponds to the absolute value of the correlation value. It can be noted that for the cases of type A, type B and type C the correlation value is relatively not so high in the entire three-dimensional region, while in type D the correlation becomes much greater than the other types. This fact suggests that the oscillation structure of type D is significantly different from the others.

In order to pay more attention to the correlation structure, the cross-correlation

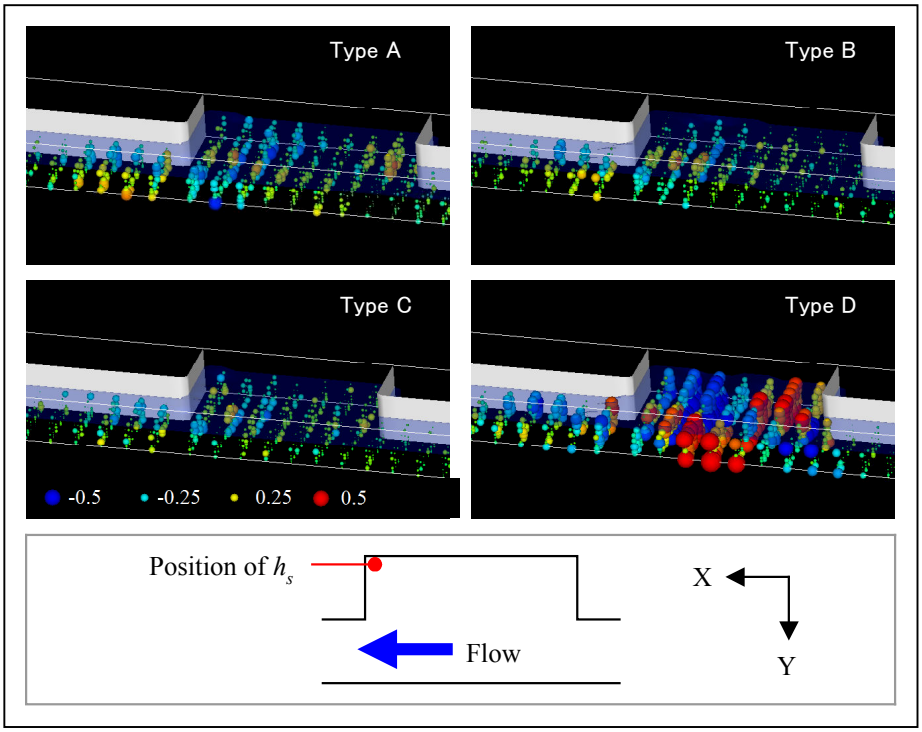

Figure 7 Cross-correlation between water depth and streamwise velocity distribution

distribution by varying the time lag dT are displayed in Figure 8 for the cases of type B and type D. It is clearly seen that in type B the larger correlation region approaches nearer to the downstream corner of the side cavity with decreasing dT. This expresses the celerity of the semi-closed seiche. On the other hand, the type D shows quite a periodic aspect of the flow and surface fields; i.e. the three dimensional correlation distributions exhibit almost the same pattern after the time lag of the predominant surface oscillation period 0.75s. In addition, almost at the opposite phase of the oscillation for dT=0.30s, the correlation distribution shows the inverse feature within the region. This suggests that a significant resonance between surface fluctuation field and the velocity field is generates in type D.

Three dimensional pathline structure

To examine the three-dimensional flow structure, three kinds of conditional sampling of velocity field is performed for the case of type D and the three dimensional pathlines for each case are indicated in Figure 9. The left figure is the result for the moment the water depth h_s is greater than the average and the right figure lower than the average. The central figure shows the total average. It can be seen that intensive recirculating flow is generated at the downstream corner of the side cavity for a rising water level, while for a lowering mode

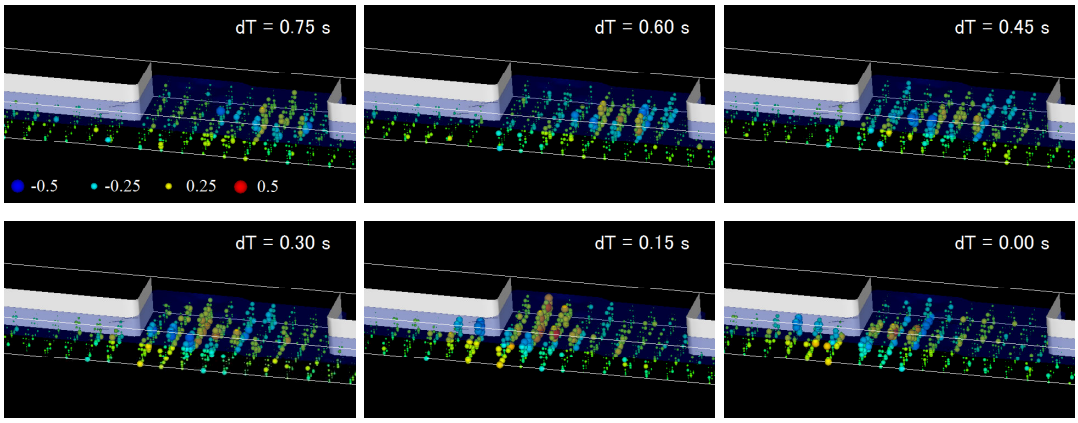

(a) Type B

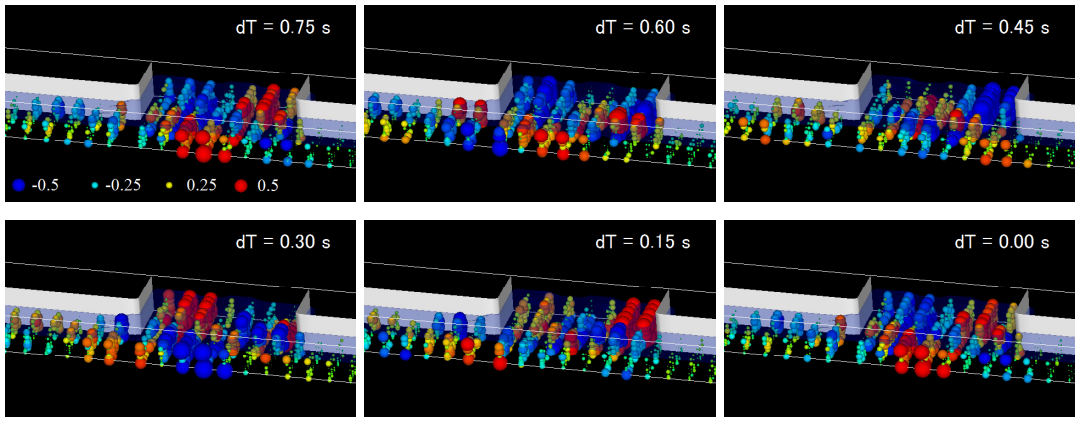

(b) Type D

Figure 8 Correlation between water depth and streamwise velocity distribution for different phases

its intensity decreases significantly. This suggests that the structure of the circulatory flow within the side cavity zone changes dynamically depending on the mode of water surface oscillation, which can be a cause of the generation of local peaks shown in Figure 4.

5. CONCLUSIONS

In this research, reliability of an LES model developed for simulating water surface oscillations within a side cavity zone was evaluated through the comparison with the experimental data obtained by image analysis. It was revealed that the categorized four types of oscillation have their own features and the most active oscillation is generated in type D. It should be noted that a slight change of side cavity length yielded a dramatic change of surface oscillation and most of those differences were successfully reproduced by the developed simulation model. From the river engineering point of view, the surface oscillation that appeared in type D would have to be avoided in the channel design, because this type of oscillation generates relatively large rise of from the mean water level on the opposite side of the side cavity as well as within the side cavity zone. For this purpose, more general description of the criteria for each type of oscillation is required in the future research.

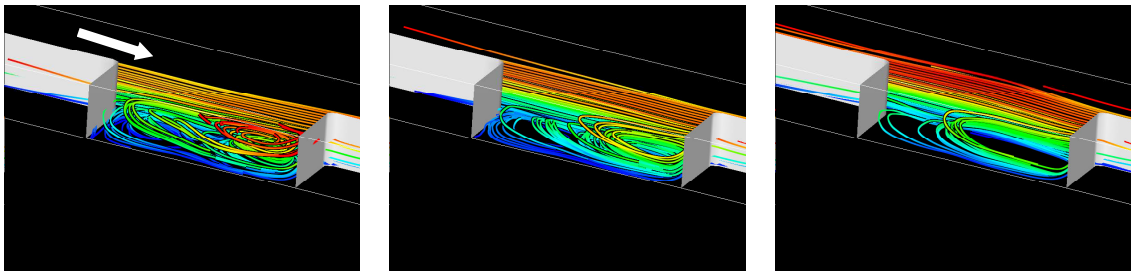

Case Fr08L30b10 h_s-plus | Case Fr08L30b10 Average | Case Fr08L30b10 h_s-minus

Figure 9 Three-dimensional flow patterns under different conditional sampling

REFERENCES

Kadotani, K., Fujita, I. and Tsubaki, R. (2008), An examination of driving force of water surface oscillation at open-channel side cavity flow, Annual Journal of Hydraulic Engineering, JSCE, 52, pp.757-762 (in Japanese).

Kimura, I. and Hosoda, T. (1997), Fundamental properties of flows in open channel with dead zone, J. Hydraulic Eng., ASCE, Vol.123, pp.98-107.

Fujita, I. , Ozawa, J. and Nagahama, K.(2001), Hydraulic characteristics of open-channel flow with a side concavity, Advances in Fluid Modelling & Turbulence Measurements (Proceeding of the 8th International Symposium on Flow Modeling and Turbulence Measurements)(FMTM2001) ,pp.39-46.

Fujita,I. and Tsubaki, R. (2005), Water surface oscillation analysis of side cavity flow using stereoscopic image measurement and POD, Annual Journal of Hydraulic Engineering, JSCE, Vol.49, pp.535-540. (in Japanese)

Rossiter, J.E. (1964), Wind-tunnel experiments on the flow over rectangular cavities at subsonic and transonic speeds, Aeronautical Research Council Reports and Memoranda, No.3438.

Tsubaki, R. and Fujita, I. (2004), Estimation of flow past a side cavity using a finite volume method with an unstructured grid, Proceedings of the Sixth International Summer Symposium, p.149-152.

Tsubaki, R. and Fujita, I. (2005), Stereoscopic Measurement of a Fluctuating Free Surface with Discontinuities, Measurement Science and Technology, Vol.16, pp.1894-1902.

Yano, M and Nezu, I. (2004), PIV measurements and LES calculations of open-channel flow with a side-cavity, Journal of Applied Mechanics, JSCE, Vol.7, pp.961-968. (in Japanese)